



# A New Step-based Photoreactor for Degradation of Acid Dye using N-TiO<sub>2</sub>-P25-coated Ceramic Foam under Visible Light

Somayeh Alijani<sup>a,\*</sup>, Mohammad Vaez<sup>b</sup>, Abdolsamad Zarringhalam Moghaddam<sup>b</sup>

a. Energy and Environment Research Center, Niroo Research Institute, Tehran, Iran  
b. Department of Chemical Engineering, Tarbiat Modares University, Tehran, Iran

Received: 2 October 2018, Revised: 17 April 2019, Accepted: 21 May 2019  
© University of Tehran 2019

## Abstract

In the present study, a new step-based photoreactor was presented to investigate the degradation of Acid Red 73 under visible light irradiation. Four N-TiO<sub>2</sub>-coated alumina foams prepared by the modified sol-gel process were arranged in each step as photocatalyst. The experimental design methodology was employed to assess the interaction between the operational parameters in the step-based photoreactor. The effect of the initial dye concentration and the dipping time of the support on degradation efficiency is highly significant. The optimal values were found to be a flow rate of 587.96 mL/min, an initial dye concentration of 5.82 mg/L, an H<sub>2</sub>O<sub>2</sub> concentration of 1.26 mg/L and the dipping time of 43 min. The 94% reduction in the chemical oxygen demand (COD) value indicated the effective mineralization of organic reactants of the solution. The kinetics analysis shows that the photocatalytic removal of Acid Red 73 in such photoreactor follows a first-order model. It was also shown that the proposed modified photoreactor could improve the degradation efficiency compared to the conventional step photoreactor. Results indicate that there is a potential to develop thin film coatings integrated into this new step-based photoreactor, allowing an effective photocatalytic process.

## Keywords:

Immobilization on Alumina Foam, N-TiO<sub>2</sub>-P25 Nanoparticles, Response Surface Methodology, Step-Based Photoreactor, Wastewater Treatment

## Introduction

Semiconductor photocatalytic technology using TiO<sub>2</sub> has been proved as an efficient method for the treatment of a wide range of organic water contaminants owing to its ability to mineralize them at atmospheric pressure and room temperature into CO<sub>2</sub> and H<sub>2</sub>O [1]. Besides the degradation of a variety of recalcitrant organics, the TiO<sub>2</sub> catalyst is relatively inexpensive, non-toxic and stable thermally and chemically [2]. However, large-scale water treatment using TiO<sub>2</sub> still experiences some limitations [3]. An efficient design of photoreactor is a key consideration which can improve the feasibility of using TiO<sub>2</sub>-based photocatalysis in practical applications [4]. The slurry type photoreactor is the most common configuration in the lab scale. This

\* Corresponding author  
E-mail: salijani@nri.ac.ir (S. Alijani)

configuration offers a high surface area for adsorption of pollutants since it uses a slurry/suspension of TiO<sub>2</sub> nanoparticles [3,5]. However, the problem of separation of the catalyst from the treated water in such design has led to developing a new type of photoreactors in which the catalyst is immobilized on a solid surface [6,7]. Though fixed-bed configurations lead to the increased lifetime of catalyst and the decreased operational cost, they experience mass transfer limitations over the immobilized layer of photocatalysts [8].

In order to reduce mass transfer limitations and promote the accessibility of contaminants to TiO<sub>2</sub>, immobilized photoreactors with various designs have been proposed [6,9,10]. Damodar and Swaminathan [6] used the immobilized TiO<sub>2</sub> rotating surfaces immersed in continuously flowing wastewater. It was shown that the rotation of coated surfaces improved mass transfer oxygen from the air and the presence of dye solution in the form of a film over the catalyst enhanced the penetration of UV radiation. Chan et al. [8] presented the cascade reactor and studied its performance in terms of photodegradation of benzoic acid. Nine TiO<sub>2</sub>-coated stainless steel plates were used under UV light and solar radiation in their research. It was found that the cascade design increased the turbulence in the flow and minimized the mass transfer resistance, while the transfer of oxygen into the solution can also be enhanced through the “waterfall” effect. In another work, Damodar et.al [7] presented a reactor consisted of a TiO<sub>2</sub>-coated glass plate located at an angle of 36° from the horizontal position. It was reported that this reactor would be an excellent design due to its simple construction, ease of operation and low fabrication cost. However, results show that the color removal in such a reactor would require longer treatment when the flow rate increases due to the decreased residence time.

Guillard et.al [11] proposed a new solar STEP photoreactor consisted of 21 steps coated by TiO<sub>2</sub> nanoparticles immobilized on the paper. They compared its performance with a CPC pilot plant photoreactor for indigo carmine and Congo red degradation. Such falling film photoreactor provided the solution with the effective transfer of oxygen and decreased the mass transfer limitation. However, they concluded that a longer time was required for the treatment of both dyes.

In this study, for the first time, a new reactor based on the step design was developed for the degradation of Acid Red 73 under visible light irradiation. A weir in each step was considered to prolong the residence time of the solution in each step improving contact between all constituents of the systems. It would, in turn, lead to the enhancement of the photocatalytic performance.

In addition to the design of photoreactor, the type of support which was integrated into the step-based photoreactor for the first time could be considered as another novelty of this study. In the present work, the reticulated alumina foam was used as the support in each step. The open 3D structure of foams minimized the mass transfer limitations by increasing the flow turbulence [12]. Our previous works demonstrated the effective photocatalytic performance and good stability of photocatalyst immobilized on alumina foam compared to the slurry system [12,13]. In addition, our previous results show that the simultaneous incorporation of nitrogen and P25 into the TiO<sub>2</sub> structure enhances TiO<sub>2</sub> activity under Visible light improving its usability under the sunlight. Therefore, it could be used as an efficient catalyst for practical applications in water treatment [13]. As a result, in this work, the N-TiO<sub>2</sub>-P25 nanopowders immobilized on the ceramic alumina foam were arranged in each step of the photoreactor as photocatalyst. These nanoparticles were synthesized by the P25 powder modified sol-gel (PPMSG) method. The photoactivity of the as-prepared film in a new-step based photoreactor was investigated using Acid Red 73 as a model contaminate under visible light radiation.

Acid Red 73 is included in the azo dye categories which have been reported as one of the most important sources of water pollution in pharmaceutical, food colorants, cosmetic, textile and printing industries [14] and there is no report indicating its degradation in such reactor system under visible light, till now.

On the other hand, to scale up a photoreactor system with effective performance, it is required to optimize a photoreactor in terms of the operational parameters [3]. In the present study, the influence of operational parameters, including initial dye concentration, flow rate, H<sub>2</sub>O<sub>2</sub> concentration, and dipping time of support on the photodegradation was studied using such a specifically designed reactor. Response surface methodology (RSM) based on the central composite design (CCD) was applied to assess the possible interactions between the influencing factors and identify their optimum levels for enhancement of photocatalytic removal of Acid Red 73 in the reactor with step-based design. Under optimum conditions, the Acid Red 73 degradation was compared in the step-based photoreactor with and without weir in each step (i.e. conventional design). The kinetics of photodegradation of Acid Red 73 was also investigated in the step-based photoreactor under visible light illumination.

## Experimental

### Materials

The following commercial reagents were used without any further purification: tetraisopropyl orthotitanate (TTIP, Ti(O-i-C<sub>3</sub>H<sub>7</sub>)<sub>4</sub>, purity 98%) as the titanium source, anhydrous ethanol (EtOH, 98%), urea (NH<sub>2</sub>CONH<sub>2</sub>) as the nitrogen precursor and TiO<sub>2</sub> P-25 nanopowder (Evonik; 50 m<sup>2</sup>/g; 80% anatase:20% rutile. Acid Red 73 (C<sub>22</sub>H<sub>14</sub>N<sub>4</sub>Na<sub>2</sub>O<sub>7</sub>S<sub>2</sub>, Mw = 556.48 g/mol), as a model acid dye, was prepared by Ciba company. All chemicals used in this work were provided by Merck.

### Synthesis of N-TiO<sub>2</sub>-P25 Catalyst and Coating on Alumina Foam

In the present work, N-TiO<sub>2</sub> nanoparticles were prepared by the P25 modified sol-gel method (PPMSG) according to our previous work [13]: A 0.25 M solution of titanium isopropoxide (TTIP) was prepared by dissolving a certain amount of TTIP in a 50 ml of anhydrous ethanol. After stirring for 30 min, a homogeneous solution was obtained. Then, the pH of the solution was adjusted below 2 by adding the mixture containing deionized water and dilute nitric acid to this solution. The acid stabilized the sol. Then, the solution with 0.73 M of urea concentration was added dropwise (30 drop/min) during vigorous stirring. After stirring for 375 min, 39.76 g/L of P-25 powder was added ultrasonically to prevent the formation of large agglomerates and prepare N-TiO<sub>2</sub> sol modified with P-25 powder. It is worth mentioning that all synthesis parameters in this work were used at their optimal values based on the results obtained from our previous works [12,13].

In this work, the reticulated macroporous alumina foams with 10 pores per inch (10 PPI) were purchased from M.S.A company to be applied as the support for the prepared N-TiO<sub>2</sub>-P25 photocatalysts. The dimensions and thickness of these foams were 95 mm × 45 mm and 10 mm, respectively. The XRD results from the previous works indicated that no noticeable change in the crystal lattice of TiO<sub>2</sub> could be detected due to the immobilization on the alumina foam [12,13]. As shown in Fig. 1a, the macrostructure of 10 PPI ceramic foam substrates provide an open three-dimensional structure, allowing the light penetration into the surface coated film.

This porous ceramic structure is also aimed at facilitating the minimization of the mass transfer limits by increasing the turbulence of the flow [15]. Therefore, in the current study, the alumina foam was used as a support for the immobilization of the N-TiO<sub>2</sub>-P25 nanoparticles.

Moreover, Fig. 1b shows the presence of microcracks in the N-doped TiO<sub>2</sub> film immobilized on alumina foam. As discussed in our previous work, it can be attributed to the presence of P25 nanoparticles incorporated into the sol [13]. The results obtained from the previous study demonstrated that these microcracks affect positively on the photoactivity by enhancing the accessibility of photons to the TiO<sub>2</sub> in the inner layers [13].

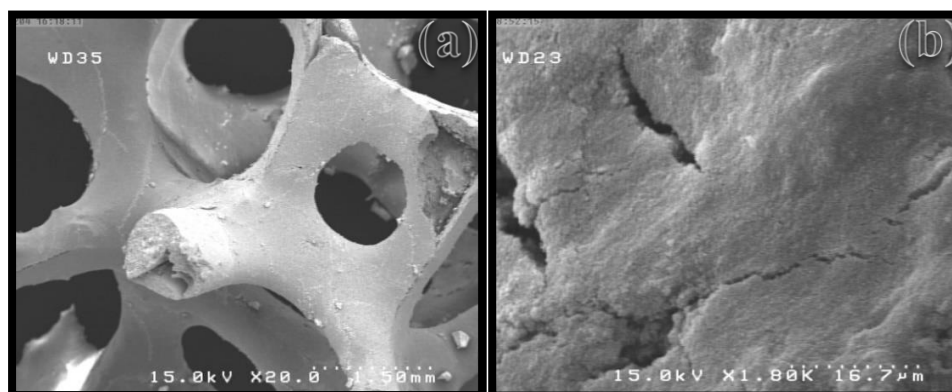


**Fig. 1.** FESEM images of the surface of Alumina foam with a pore size of 10 PPI (a) Alumina foam coated by N-TiO<sub>2</sub>-P25 film prepared at optimal conditions (b)

**Table 1.** Experimental range and levels of the independent test variables

Variables	Ranges and levels				
	-2	-1	0	+1	+2
Flow rate (mL/min) ( $x_1$ )	200	400	600	800	1000
Initial dye concentration (mg/L) ( $x_2$ )	5	7.5	10	12.5	15
H <sub>2</sub> O <sub>2</sub> concentration (mg/L) ( $x_3$ )	0.5	0.88	1.25	1.63	2
Dipping time of support into the sol (min) ( $x_4$ )	10	22.5	35	47.5	60
Q (min)	1	2	3	4	6
R (min)	0	2.5	5	7.5	0

Therefore, in this work, the N-TiO<sub>2</sub> nanoparticles were prepared by the P25 modified sol-gel method at first, followed by immobilization on the alumina foams as film and then, arranged in the step-based photoreactor as photocatalyst.

In this work, the dipping time of support into the sol was considered as an independent variable ranging from 10 to 60 min (Table 1). Dividing the time value by 10, the quotient and remaining values were considered as Q and R, respectively.

In order to perform the dipping process for a certain time, the N-TiO<sub>2</sub>-P25 was coated on the substrate by dipping the alumina foam into the sol for 10 min, followed by a drying process at 80 °C for 10 min. The number of repetition of this process was equal to the value of Q. Then, the support was dipped into the sol for R min and the drying process was carried out at 80 °C for 10 min. The final samples were produced by the calcination at 400 °C for 1 h, with a heating and cooling rate of 1 °C/min. It is known that the dipping time of the support into the N-TiO<sub>2</sub>-P25 sol affects the catalyst loading. In order to identify the loading of N-TiO<sub>2</sub>-P25 immobilized on the alumina foam at the different dipping time, foams were washed with acetone and subsequently with distilled water. After drying the foams at 100 °C for 2 h, the weight of foams was measured. Then, the coating process of N-TiO<sub>2</sub>-P25 on the alumina foam was carried out at the different dipping time as the procedure explained before. The difference of the foam weight before and after the coating process was considered as the N-TiO<sub>2</sub>-P25 loading on the substrate with a certain dipping time. Table 2 shows the catalyst loading measured at the different dipping time of the support into the N-TiO<sub>2</sub>-P25 sol. As data shown in Table 2, the N-TiO<sub>2</sub>-P25 loading immobilized on the alumina foam increases with prolonging the dipping time of the support. It could influence the photocatalytic performance of the resulting samples, as discussed later.

### Experimental Setup and Photocatalytic Activity Measurement

Fig. 2 shows a schematic diagram of the photoreactor used in this work. The apparatus was composed of a rectangular box (510 mm × 210 mm) made of Plexiglas with 260 mm height having 4 steps. The four alumina foams coated with N-TiO<sub>2</sub>-P25 film were positioned in each

step. An air pump with a 1 L/min flow rate aerated the dye solution in the steps. A solution contained the known values of  $\text{H}_2\text{O}_2$  and Acid Red 73 ( according to Table 1), was fed into the reservoir tank and flowed down by a distributor through the reactor as a thin layer. The presence of  $\text{H}_2\text{O}_2$  in the solution, as a supplement additive for oxidation, can provide additional hydroxyl radicals for improvement of the removal process of organic pollutants in the degradation of Acid Red 73 [8]. An aquarium pump (RESUN, SP-880) was used to recycle the solution. A flowmeter was employed to adjust the flow rate of the solution according to Table 1, and the temperature of the solution was controlled by a temperature bath (WEIPRO, MT-10). 4.5 liters of dye solution was treated in all the experiments. To reach the complete equilibrium of adsorption process in each experiment, the dye solution contained catalyst was circulated in the darkness for 60 min. For this purpose, the experimental setup was kept in a box covered with a roll of aluminum foil. A 300 W halogen lamp (Osram) with the wavelength between 400 to 800 nm was applied as a visible light source. In order to filter UV light and excite samples only by visible light, a UV cut-off filter was used. The sampling was conducted at certain time intervals during 120 min of radiation time, and any possible titania nanoparticles existing in the sample was removed using a centrifuge (Hettich, EBA 20). Then, an Optizen 3220UV Double Beam spectrophotometer was employed to measure the residual concentration of Acid Red 73 at the maximum wavelength ( $\lambda_{\text{max}} = 545 \text{ nm}$ ).

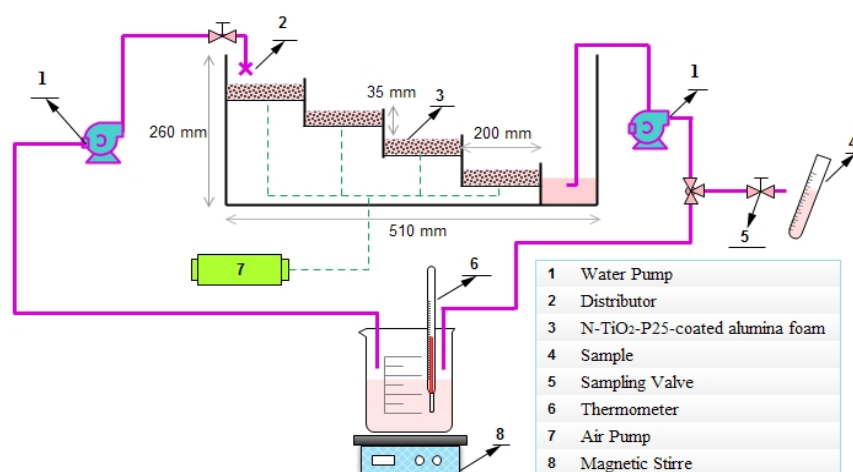


Fig. 2. Schematic diagram of the cascade-based photoreactor

Table 2. Catalyst loading on the alumina foam at different dipping time of the support

Dipping time of the support into the N-TiO <sub>2</sub> -P25 sol (min)	Catalyst loading (wt.%)
10	3.3
22.5	7.4
35	10.1
47.5	15.2
60	21

### Experimental design and optimization by Response Surface Methodology

A five-level central composite design (CCD), as the most usual form of the experimental design, was applied to assess the simultaneous impact of operational variables and identify their optimal values for degradation of Acid Red 73 in the photoreactor with the step-based design. The effect of four independent variables (flow rate ( $x_1$ ), initial dye concentration ( $x_2$ ),  $\text{H}_2\text{O}_2$  concentration ( $x_3$ ) and dipping time of support into the sol ( $x_4$ )) was investigated in the reactor through 30 runs of experiments, while the photodegradation efficiency of Acid Red 73 was considered as the dependent parameter (response). All experimental runs were conducted at the room temperature according to Table S1 in the Supplementary information.

Following, there is an empirical second-order polynomial model, applied to fit the results of CCD.

$$Y(\%) = b_0 + b_1x_1 + b_2x_2 + b_3x_3 + b_4x_4 + b_{12}x_1x_2 + b_{13}x_1x_3 + b_{14}x_1x_4 + b_{23}x_2x_3 + b_{24}x_2x_4 + b_{34}x_3x_4 + b_{11}x_1^2 + b_{22}x_2^2 + b_{33}x_3^2 + b_{44}x_4^2 \quad (1)$$

where Y is the response variable (degradation efficiency), and  $x_i$ 's are the independent variables. Also  $b_i$  and  $b_{ii}$  indicate the regression coefficients of linear and quadratic effects, respectively and  $b_{ij}$ 's imply to the interaction coefficients of factors. The Design Expert 7.0 software was applied for the analysis of the experimental results.

### Analytical Procedures

#### *Chemical Oxygen Demand Analysis*

The digestion of a mixture of 3 mL of degraded sample and the reagents was carried out for 2 h at 423 K using a Spectroquant TR320 thermo digester. After cooling the mixture at the room temperature, the chemical oxygen demand (COD) of the samples were measured.

#### *Kinetic Studies*

Kinetic studies on the photocatalytic processes of water pollutants are useful for process scale-up presenting an optimal design of the photoreactor system with sufficient capacity [3]. In this work, The kinetic studies were performed at 25 °C to assess the impact of the initial acid red concentration on the photodegradation. An immobilized N-TiO<sub>2</sub>-P25 step-based photoreactor with Acid Red 73 solution (5-15 mg/L) at pH of 6.5 was used. The flow rate, H<sub>2</sub>O<sub>2</sub> concentration and the dipping time were fixed at 600 mL/min, 1.25 mg/L and 35 min, respectively.

## Results and discussions

### The Effect of Nitrogen and P25 Nanoparticles

In this work, urea was used as the nitrogen precursor for the incorporation of N atoms in the TiO<sub>2</sub> structure. Based on the diffuse reflectance spectra (DRS) analysis of the differently prepared samples, it was demonstrated that the presence of nitrogen in the crystalline lattice of titania induced a shift in the absorption band towards the visible regions (Fig. 3c and b). The band gap energy for N-TiO<sub>2</sub> and N-TiO<sub>2</sub>-P25 catalysts were found to be 2.15 and 2.08 eV, respectively. Similar results have been reported in our previous work [13]. It must be noted that this shift is only attributed to the nitrogen doping not to the presence of P25 particles since the undoped samples (Fig. 3a and b) presented no photon-response in the visible region.

In addition to the optical properties of TiO<sub>2</sub>, the nitrogen made also an impact on the particle size of the catalysts obtained, as BET analysis shown in our previous work [13]. The results indicated that the specific surface area of the samples increased from 25.58 to 38.40 m<sup>2</sup>/g with nitrogen doping due to the prevention of crystal growth in the presence of nitrogen. Therefore, in the present work, nitrogen doping was applied as an approach for inducing the photoactivity of TiO<sub>2</sub> in the step-based reactor under visible light.

On the other hand, as shown in Fig. 1b, the incorporation of P25 powder into the sol leads to the formation of microcracks enhancing the light permeability to the inner layers. According to the photoactivity of the different films (Fig. 4a and b), the films contained P25 powder reveal higher photoactivity comparing to those made without P25 nanoparticles (i.e. typical sol-gel technique). Hence, such results confirm the positive effect of the microcracks present in the films contained P25 nanopowders [12,13]. In addition to the P25 nanoparticles, the photocatalytic performance of the as-prepared films was also affected by the incorporation of

the nitrogen into the film. As seen in Fig. 4a, b, and c, the N-TiO<sub>2</sub>-P25 films exhibit a higher photoactivity compared with those contained P25 nanoparticles only. This can be attributed to the impact of nitrogen on the optical properties and specific surface area of the samples, as BET and DRS results shown. Generally, the effect arising from both nitrogen and P25 nanoparticles resulted in the higher Vis activity of the films containing both nanoparticles.

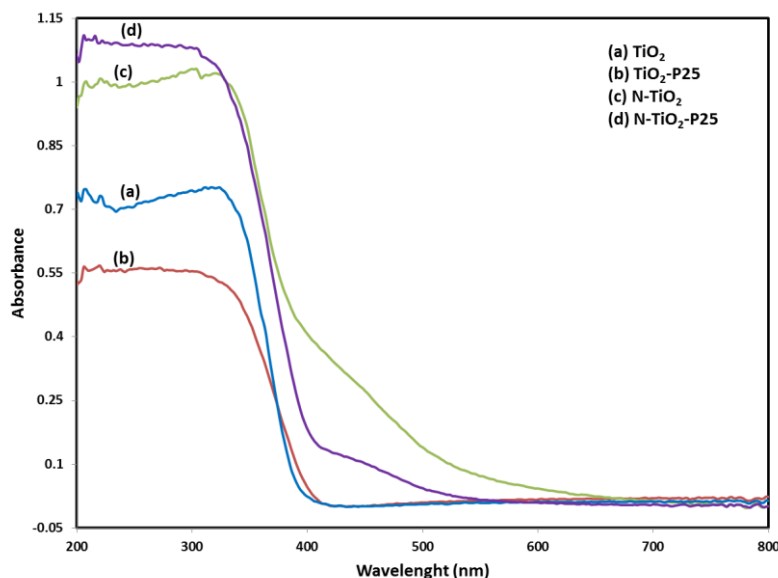


**Fig. 3.** UV-vis DRS spectra for (a) pure TiO<sub>2</sub> (b) TiO<sub>2</sub>-P25 (c) N-TiO<sub>2</sub> (d) N-TiO<sub>2</sub>-P25 samples

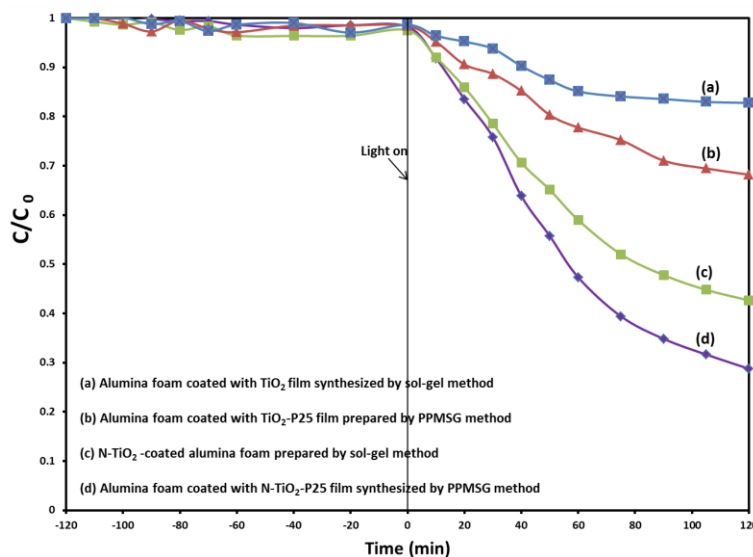


**Fig. 4.** Effect of photocatalyst on the degradation of Acid Red 73 under visible light (initial concentration of dye: 10 mg/L, pH: 6.5 and concentration H<sub>2</sub>O<sub>2</sub>: 0.55 mg/L)

## Mathematical Model Analysis

### *Model Fitting and Analysis of Variance (Anova)*

The predicted responses obtained from polynomial regression equations together with the experimental results obtained from the design matrix are presented in Table S1 in the Supplementary information. Based on the obtained results, the following polynomial regression equation was generated by the Design Expert software, which expresses the empirical relationship between independent variables and the response in the actual form:

$$\begin{aligned} \% \text{Degradation} = & -160.54375 + 0.09652v + 10.23167[\text{Dye}] + 103.18889[\text{H}_2\text{O}_2] + 4.21833t - \quad (2) \\ & 1.125 \times 10^{-3}[\text{Dye}]v + 0.045833[\text{H}_2\text{O}_2]v - 7.25 \times 10^{-4}vt - 1.4[\text{Dye}][\text{H}_2\text{O}_2] - 0.034[\text{Dye}]t - \\ & 0.28[\text{H}_2\text{O}_2]t - 9.92187 \times 10^{-5}v^2 - 0.51500[\text{Dye}]^2 - 42.44444 [\text{H}_2\text{O}_2]^2 - 0.039t^2 \end{aligned}$$

where  $v$  refers to flow rate,  $[\text{Dye}]$  is the initial dye concentration,  $[\text{H}_2\text{O}_2]$  indicates  $\text{H}_2\text{O}_2$  concentration and  $t$  is the dipping time of the support into the sol. The negative coefficients of the second-order terms  $x_{ii}^2$  in the polynomial equation indicate that an excessive value of the independent variables of the system led to a decrease in the degradation efficiency.

The adequacy of the model was evaluated by the analysis of variance (ANOVA). The  $p$ -value obtained for the model is less than 0.0001 (Table 3), which indicates that the model is significant. The model  $F$ -value of 57.46 also implies that the model is significant and there is only a 0.01% chance that the “model  $F$  value” could occur due to noise.

**Table 3.** ANOVA results for the response surface quadratic model

Source	Sum of squares	Degree of freedom	Mean squares	F value	P value
Model	4833.45	14	345.25	57.46	<0.0001
Residual	90.12	15	6.01	-	-
Lack of fit	81.25	10	8.12	4.58	0.0535
Pure error	8.88	5	1.78	-	-
Total	4923.57	29	-	-	-

The “lack-of-fit  $F$ -value” of 4.58 indicates that the lack of fit is insignificant relative to the pure error. Based on the results shown in Table 3, there is a 5.35% chance that the “lack-of-fit  $F$ -value” could occur due to noise. Such results verify the ability of the model to predict the experimental findings accurately. The value of “pred  $R$ -Squared” of 0.9024 which reasonably agrees with the value of “adj  $R$ -Squared” of 0.9646, also proves the adequate ability of the model for prediction of experimental results.

Table S2 of the Supplementary information displays the ANOVA results at 95% confidence levels. According to the  $p$ -value, as a tool for evaluation of the significance level of parameters, the initial dye concentration ( $x_2$ ), the dipping time of support into the sol ( $x_4$ ), the interaction effect between the flow rate and  $\text{H}_2\text{O}_2$  concentration ( $x_1x_3$ ), the interaction effect between the flow rate and the dipping time ( $x_1x_4$ ) and the second-order effect of variables ( $x_{ii}^2$ ) are highly significant factors with  $p$ -value less than 0.001. Moreover, the impact of the interaction between the initial dye concentration and  $\text{H}_2\text{O}_2$  concentration ( $x_2x_3$ ) and the simultaneous effect of the  $\text{H}_2\text{O}_2$  concentration and dipping time ( $x_3x_4$ ) is significant with  $p < 0.05$ . In addition, the model variable is insignificant with the  $p$ -value larger than 0.05. According to data of Table S2 of the Supplementary information, the effect of the flow rate and  $\text{H}_2\text{O}_2$  concentration are insignificant for Acid Red 73 degradation in the step-based photoreactor under visible light.

Based on the values of the monomial coefficients derived from the model,  $p(x_1) = 0.4652$ ,  $p(x_2) < 0.0001$ ,  $p(x_3) = 0.5686$  and  $p(x_4) < 0.0001$ , the decreasing order of the influence of independent variables on Acid Red 73 degradation in the step-based photoreactor is initial dye concentration > dipping time of the support into the sol > flow rate >  $\text{H}_2\text{O}_2$  concentration. It must be noted that the obtained ranking can be related to the experimental range of independent parameters studied in this work.

### Response Surface Analysis

In order to have a better understanding of interactions between variables, the response predicted by the model can be presented graphically in three-dimensional plots [16]. This effective graphical tool is also extensively applied to find the optimal value of variables. The changes in

degradation efficiency (response) in terms of the interactions between independent variables are shown in Fig. 5.

Fig. 5a shows the effect of the flow rate and H<sub>2</sub>O<sub>2</sub> concentration simultaneously on the photocatalytic removal of Acid Red 73. Degradation increases gradually with increasing flow rate from 200 to 600 mL/min and decreases drastically when the flow rate increases beyond 600 mL/min. The positive impact of flow rate can be ascribed to the increased turbulence in the system and the enhanced mass transfer coefficient, leading to the decomposition of more adsorbed dye molecules on the catalyst surface [17]. The decreased photodegradation at the higher flow rate can be ascribed to the decreased contact time between the solution of reactants and the surface of catalyst as reported in the literature [7,17,18]. In addition, it has been reported that at very high flow rates, there may be inadequate generated hydroxyl radicals for oxidation of the high load of dye. This would result in poor photocatalytic removal [6].

However, the high concentration of H<sub>2</sub>O<sub>2</sub> slows down the negative impact of the flow rate on the photocatalytic degradation, as shown in Fig. 5a. This behavior may be attributed to the role of H<sub>2</sub>O<sub>2</sub> as an inhibitor of the recombination of hole-electron by accepting the electron from the conduction band which has a positive impact on the photocatalytic performance [19-21].

The effects of the flow rate and dipping time on the degradation of Acid Red 73 under visible light are shown in Fig. 5b. As the dipping time of the support into the sol increases, the degradation of dye increases extremely, confirming the positive influence of the increased number of N-TiO<sub>2</sub> active sites [22]. However, at the longer dipping time (>40min) and consequently higher catalyst loading, a slight reduction in acid dye degradation is observed. This observation can be explained by the reduction of light permeability and unavailability of organic pollutants to the N-TiO<sub>2</sub> particles in the inner layers [23,24]. As results shown in Fig. 5b, the high flow rate accelerates the negative effect of dipping time on the color removal efficiency due to the decreased residence time of the solution per pass.

Fig. 5c shows the effects of H<sub>2</sub>O<sub>2</sub> concentration and the dipping time of the substrate on photodegradation. By increasing H<sub>2</sub>O<sub>2</sub> concentration in the system, the photocatalytic performance increases up to a maximum value and afterward decreases gradually. The positive impact of H<sub>2</sub>O<sub>2</sub> concentration on photodegradation can be ascribed to the role of H<sub>2</sub>O<sub>2</sub> as a conduction band electron acceptor and a source of OH<sup>•</sup> [21,25]. H<sub>2</sub>O<sub>2</sub> serves two roles in photocatalysis reaction leading to improvement of photocatalytic activity. It can act as a source of dissolved oxygen by decomposing into oxygen, as indicated in the following reaction [8]:



Dissolved oxygen plays a key role in the inhibition of the recombination of the electron-hole pair by providing sufficient electron scavengers [3]. In addition, hydrogen peroxide could favor the dissolved oxygen level and maintain the photoactivity, through the following mechanisms [3,21]:



At high concentration, hydrogen peroxide consumes the hydroxyl radicals and the valence band holes (reactions 3-5) leading to a poor photocatalytic removal [8,19].



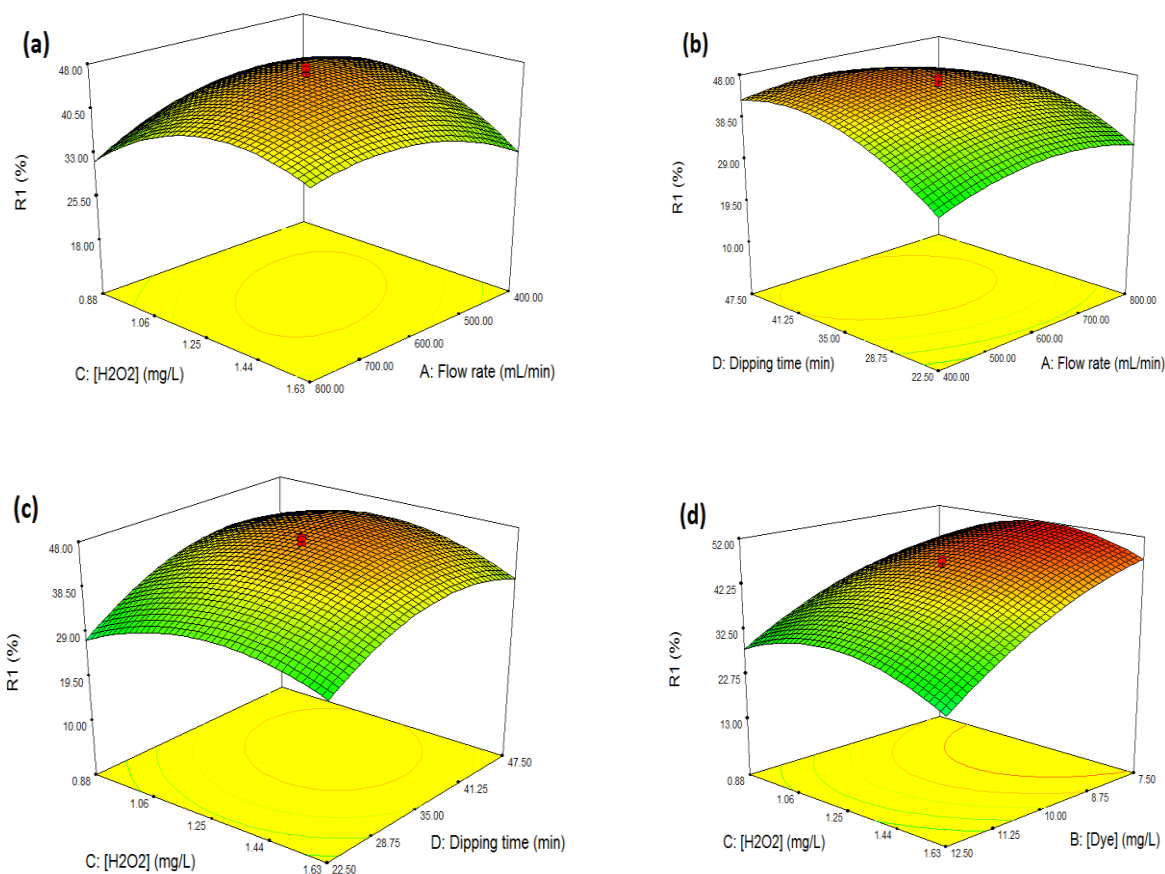


**Fig 5.** Effects of flow rate and  $\text{H}_2\text{O}_2$  concentration on Acid Red 73 degradation ( dye: 10 mg/L and dipping time: 35 min) (a) Effects of flow rate and dipping time on the Acid Red 73 degradation efficiency (dye: 10 mg/L and  $\text{H}_2\text{O}_2$  concentration: 1.25 mg/L) (b) Effects of  $\text{H}_2\text{O}_2$  concentration and dipping time on the Acid Red 73 degradation efficiency ( flow rate: 600 mL/min and dye: 10 mg/L) (c) Effects of  $\text{H}_2\text{O}_2$  concentration and initial dye concentration on the Acid Red 73 degradation efficiency ( flow rate: 600 mL/min and dipping time: 35 min)

However, as seen in Fig. 5c, longer dipping time declines the negative effect of  $\text{H}_2\text{O}_2$  concentration on the Vis activity of the catalyst. The enhanced loading of catalyst at the samples prepared with longer dipping time can be responsible for this observation. It is also noted that the influence of dipping time on the degradation of Acid Red 73 is significantly higher than the effect of  $\text{H}_2\text{O}_2$  concentration on the photodegradation (Table S2 in the Supplementary information). Therefore, the photocatalytic performance is affected by the dipping time rather than  $\text{H}_2\text{O}_2$  concentration, when both parameters changes.

The effects of the initial dye concentration and  $\text{H}_2\text{O}_2$  concentration on the photodegradation of Acid Red 73 are shown in Fig. 5d. The effect of  $\text{H}_2\text{O}_2$  concentration on the photocatalytic removal of dye exhibited the trend as explained earlier. At higher concentration of dye, the competitive adsorption of the parental dye and intermediates accelerates the negative effect of  $\text{H}_2\text{O}_2$  concentration on the photocatalytic performance. Moreover, at higher dye concentration, the concentration of the formed intermediates and consequently the competition between the dye and the intermediates increase leading to a decrease in the energy required for the hydroxyl generation [6]. It is also noticed that there is a highly significant effect of initial dye concentration on the degradation compared with  $\text{H}_2\text{O}_2$  concentration (Table S2 in the Supplementary information). Therefore, when these parameters changes simultaneously, the photocatalytic removal of dye is mostly influenced by the initial dye concentration.

### Optimization of operational parameters

Optimization was performed in term of the desirability function to find the optimal conditions for Acid Red 73 degradation using the N-TiO<sub>2</sub>-P25 immobilized on the alumina foam in the step-based photoreactor under visible light irradiation. The adjustments and upper/lower bounds for all variables were set according to Table S3 of the Supplementary information. Based on the given settings, the optimal values for maximum removal efficiency of Acid Red 73 (53.73%) in the step-based photoreactor were found to be a flow rate of 587.96 mL/min, an initial dye concentration of 5.82 mg/L, an H<sub>2</sub>O<sub>2</sub> concentration of 1.26 mg/L and the dipping time of 43 min. Based on the optimum value of dipping time, the dipping process was performed and the optimal loading of the catalyst was found to be 12 wt.%.

### Model Validation and Confirmation

The validity of the model for the prediction of maximum degradation of Acid Red 73 was checked using the optimal values derived from the model. An average maximum degradation of 52.67% was obtained from the experiments replicated at optimum conditions for three times. The reasonable agreement between the predicted (53.73%) and the experimental results (52.67%) proves the ability of the model for the valid simulation of the photodegradation of Acid Red 73 in the step-based photoreactor.

### Mineralization Studies

The ability of the immobilized N-TiO<sub>2</sub>-P25 step-based photoreactor for degradation of Acid Red 73 and its intermediates was investigated using COD. It must be noted that the photoreactor operated under optimal conditions in the presence of visible light. Changes in COD for the Acid Red 73 degradation are displayed in Fig. 6. The 94% reduction in the COD value is evidence of the effective performance of immobilized step-based photoreactor in the complete degradation of acid dye.

### Kinetic Analysis of Acid Red 73 Photodegradation

In order to scale up the process and design a photoreactor system with optimum capacity, kinetics studies on the photocatalytic rate of the water contaminants could be useful [3]. The kinetics of photocatalytic oxidation of organic pollutants usually follows the Langmuir-Hinshelwood (L-H) equation as given below [26]:

$$r = k_{L-H} \frac{K_{ads}[C_0]}{1 + K_{ads}[C_0]} \quad (3)$$

where  $r$  indicates the rate of reaction ( $\text{mg L}^{-1} \text{min}^{-1}$ ),  $K_{ads}$  is the adsorption coefficient of the reactant on catalyst ( $\text{L mg}^{-1}$ ),  $k_{L-H}$  represents the reaction rate constant ( $\text{mg L}^{-1} \text{min}^{-1}$ ),  $C$  is the concentration of the reactant ( $\text{mg L}^{-1}$ ) in the solution at time  $t$ , and  $t$  is the reaction time (min).

When the initial concentration of organics is low, Eq. 3 could be reduced to the pseudo-first-order reaction rate [26]:

$$r = -\frac{dC}{dt} = k_{L-H}K_{ads}C \quad (4)$$

$$\ln \frac{C}{C_0} = -k_{app}t \quad (5)$$

where  $C_0$  is the initial concentration of the reactant and  $k_{app}=k_{L-H}K_{ads}$  ( $\text{min}^{-1}$ ) could be considered as the pseudo rate constant.

Fig. 7 shows the kinetic profile of photodegradation of Acid Red 73 in the step-based photoreactor under visible light irradiation. According to the linear correlation between  $\ln(C/C_0)$  and  $t$ , the photocatalytic degradation of Acid Red 73 in the step-based photoreactor obeys the first-order kinetics. The apparent rate constant,  $k$ , was obtained from the line slope of  $\ln(C/C_0)$  versus  $t$ . By comparing the values of  $k$ , it is obvious that the photodegradation of acid dye decreases with increasing initial dye concentration, as discussed earlier.

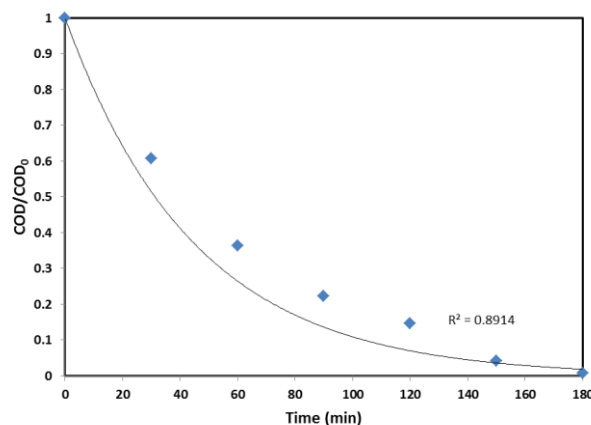


**Fig. 6.** COD removal during photocatalytic degradation of Acid Red 73 (dye: 5.82 mg/L, H<sub>2</sub>O<sub>2</sub>: 1.26 mg/L, pH: 6.5, COD<sub>0</sub>: initial COD and COD: COD at time  $t$ )

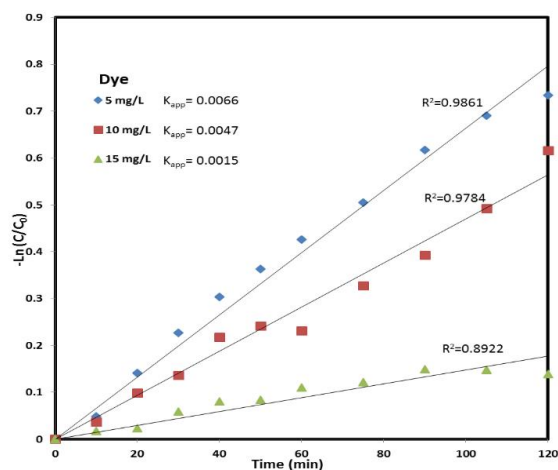


**Fig. 7.** Kinetics of photocatalytic degradation of Acid Red 73 in the step-based photoreactor under visible light irradiation (flow rate: 600 mL/min, H<sub>2</sub>O<sub>2</sub>: 1.26 mg/L, pH: 6.5 and dipping time: 35 min)

### Stability and Reusability of Photocatalytic Surface in Step-Based Photoreactor

Since the ability of the immobilized photocatalyst to be used repeatedly is a key factor for the large application, the reusability of the N-TiO<sub>2</sub>-P25-coated foam in step-based photoreactor was also evaluated in four repeated experiments. All the experiments were done under optimal conditions (flow rate: 587.96 mL/min, dye: 5.82 mg/L, H<sub>2</sub>O<sub>2</sub>: 1.26 mg/L and the dipping time: 43 min). A 100 min was considered for the time of each run. During this time, the sampling was conducted at certain time intervals to measure the residual concentration of Acid Red 73. At the end of each run, the experimental conditions were set again at the optimal conditions and the photocatalyst was reused without any recovery or purification. As shown in Fig. 8, the photoactivity decreased only by 5% after four cycles indicating the applicability of the as-prepared film in the step-based photoreactor within a long time of operation. Additionally, the stability of N-TiO<sub>2</sub>-P25 immobilized on alumina foam was also investigated by the procedure reported in our previous work [12].

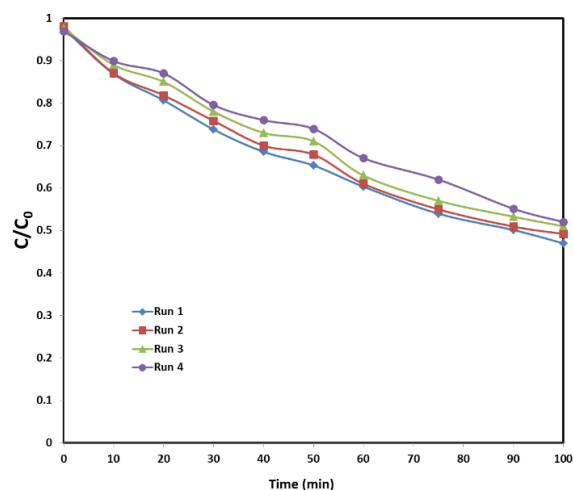


**Fig. 8.** The cyclic photocatalytic performance of N-TiO<sub>2</sub>-P25-coated alumina foam for Acid Red 73 degradation in the step-based photoreactor

### Effect of Configuration

In order to study the influence of the weir inserted in each step, the photodegradation of Acid Red 73 in the step-based photoreactor was compared to that in a step photoreactor without weir in each step. It is noted that the process was performed under optimal conditions in the presence of visible light irradiation. As seen in Fig. 9, almost no change in dye concentration observed without light radiation (dark). The negligible change in Acid Red 73 degradation was noted using alumina foam under visible light irradiation (Fig. 9a). Similar results have been also found in our previous work [13]. These results show the inactivity of the alumina foam as photocatalyst and the slight degradation of acid dye in this process can be ascribed to the presence of Vis light-H<sub>2</sub>O<sub>2</sub>.

Results obtained from three replicated experiments show that the photoreactor presented in this work is more efficient than the step photoreactor without weir in the degradation of acid dye, considering the same treatment time (Fig. 9b and c). The proposed modified photoreactor could improve the degradation efficiency by over 8%, under the optimal conditions. This result can be attributed to the presence of weir in each step which provides an enhanced contact time between the catalyst and reactants.

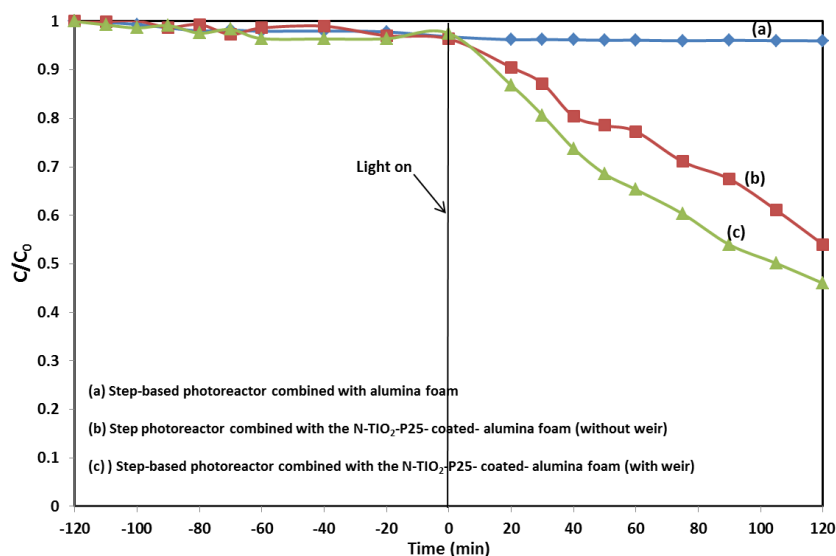


**Fig. 9.** Photocatalytic degradation of Acid Red 73 the photoreactor with different configuration operated under optimal conditions

## Conclusions

The degradation of Acid Red 73 was investigated using N-TiO<sub>2</sub>-P25- coated alumina foams arranged in a specially designed step-based photoreactor. The RSM model was applied to identify the optimal working conditions in the study of such a system for the degradation of acid dye under visible light irradiation. The step-based photoreactor working at the optimal conditions was found to be more efficient than a step photoreactor with the same time of treatment. Considering the effective photocatalytic performance of the photoreactor, it could be used as an alternative for combination with thin film in the large applications of water treatment. Based on the results obtained from the present work, the application of weir structure in step photocatalytic reactors can improve the degradation efficiency, regardless of the type of support, photocatalyst and the nature of the dye.

## Reference

- [1] He HY, Chen P. Recent advances in property enhancement of nano TiO<sub>2</sub> in photodegradation of organic pollutants. *Chemical Engineering Communications*. 2012 Dec 1;199(12):1543-74.
- [2] Vaez M, Moghaddam AZ, Mahmoodi NM, Alijani S. Decolorization and degradation of acid dye with immobilized titania nanoparticles. *Process Safety and Environmental Protection*. 2012 Jan 1;90(1):56-64.
- [3] Chong MN, Jin B, Chow CW, Saint C. Recent developments in photocatalytic water treatment technology: a review. *Water Research*. 2010 May;44(10):2997-3027.
- [4] Shan AY, Ghazi TI, Rashid SA. Immobilisation of titanium dioxide onto supporting materials in heterogeneous photocatalysis: a review. *Applied Catalysis A: General*. 2010 Dec 1;389(1-2):1-8.
- [5] Eydivand S, Nikazar M. Degradation of 1, 2-Dichloroethane in simulated wastewater solution: A comprehensive study by photocatalysis using TiO<sub>2</sub> and ZnO nanoparticles. *Chemical Engineering Communications*. 2015 Jan 2;202(1):102-11.
- [6] Damodar RA, Swaminathan T. Performance evaluation of a continuous flow immobilized rotating tube photocatalytic reactor (IRTPR) immobilized with TiO<sub>2</sub> catalyst for azo dye degradation. *Chemical Engineering Journal*. 2008 Oct 1;144(1):59-66.
- [7] Damodar RA, Jagannathan K, Swaminathan T. Decolourization of reactive dyes by thin film immobilized surface photoreactor using solar irradiation. *Solar Energy*. 2007 Jan 1;81(1):1-7.
- [8] Chan AH, Chan CK, Barford JP, Porter JF. Solar photocatalytic thin film cascade reactor for treatment of benzoic acid containing wastewater. *Water Research*. 2003 Mar 1;37(5):1125-35.
- [9] Lee JH, Nam W, Kang M, Han GY, Yoon KJ, Kim MS, Ogino K, Miyata S, Choung SJ. Design of two types of fluidized photo reactors and their photo-catalytic performances for degradation of methyl orange. *Applied Catalysis A: General*. 2003 May 8;244(1):49-57.
- [10] Rizzo L, Koch J, Belgioirno V, Anderson MA. Removal of methylene blue in a photocatalytic reactor using polymethylmethacrylate supported TiO<sub>2</sub> nanofilm. *Desalination*. 2007 Jun 10;211(1-3):1-9.
- [11] Guillard C, Disdier J, Monnet C, Dussaud J, Malato S, Blanco J, Maldonado MI, Herrmann JM. Solar efficiency of a new deposited titania photocatalyst: chlorophenol, pesticide and dye removal applications. *Applied Catalysis B: Environmental*. 2003 Nov 10;46(2):319-32.
- [12] Alijani S, Moghaddam AZ, Vaez M, Towfighi J. Characterization of TiO<sub>2</sub>-coated ceramic foam prepared by modified sol-gel method and optimization of synthesis parameters in photodegradation of Acid Red 73. *Korean Journal of Chemical Engineering*. 2013 Oct 1;30(10):1855-66.
- [13] Alijani S, Moghaddam AZ, Vaez M, Towfighi J. Synthesis of N-TiO<sub>2</sub>-P25 coated on ceramic foam by modified sol-gel method for Acid Red 73 degradation under visible-light irradiation. *Research on Chemical Intermediates*. 2015 Jul 1;41(7):4489-509.
- [14] Collazzo GC, Foletto EL, Jahn SL, Villetti MA. Degradation of Direct Black 38 dye under visible light and sunlight irradiation by N-doped anatase TiO<sub>2</sub> as photocatalyst. *Journal of Environmental Management*. 2012 May 15;98:107-11.

- [15] Ochuma IJ, Osibo OO, Fishwick RP, Pollington S, Wagland A, Wood J, Winterbottom JM. Three-phase photocatalysis using suspended titania and titania supported on a reticulated foam monolith for water purification. *Catalysis Today*. 2007 Oct 15;128(1-2):100-7.
- [16] Soleymani AR, Saïen J, Chin S, Le HA, Park E, Jurng J. Modeling and optimization of a sono-assisted photocatalytic water treatment process via central composite design methodology. *Process Safety and Environmental Protection*. 2015 Mar 1;94:307-14.
- [17] Natarajan K, Natarajan TS, Bajaj HC, Tayade RJ. Photocatalytic reactor based on UV-LED/TiO<sub>2</sub> coated quartz tube for degradation of dyes. *Chemical Engineering Journal*. 2011 Dec 15;178:40-9.
- [18] Mozia S, Tomaszewska M, Morawski AW. Decomposition of nonionic surfactant in a labyrinth flow photoreactor with immobilized TiO<sub>2</sub> bed. *Applied Catalysis B: Environmental*. 2005 Aug 8;59(3-4):155-60.
- [19] Vaez M, Zarringhalam Moghaddam A, Alijani S. Optimization and modeling of photocatalytic degradation of azo dye using a response surface methodology (RSM) based on the central composite design with immobilized titania nanoparticles. *Industrial & Engineering Chemistry Research*. 2012 Mar 7;51(11):4199-207.
- [20] Sakkas VA, Islam MA, Stalikas C, Albanis TA. Photocatalytic degradation using design of experiments: a review and example of the Congo red degradation. *Journal of Hazardous Materials*. 2010 Mar 15;175(1-3):33-44.
- [21] So CM, Cheng MY, Yu JC, Wong PK. Degradation of azo dye Procion Red MX-5B by photocatalytic oxidation. *Chemosphere*. 2002 Feb 1;46(6):905-12.
- [22] Chong MN, Jin B, Chow CW, Saint CP. A new approach to optimise an annular slurry photoreactor system for the degradation of Congo Red: Statistical analysis and modelling. *Chemical Engineering Journal*. 2009 Oct 1;152(1):158-66.
- [23] Parra S, Stanca SE, Guasaquillo I, Thampi KR. Photocatalytic degradation of atrazine using suspended and supported TiO<sub>2</sub>. *Applied Catalysis B: Environmental*. 2004 Jul 30;51(2):107-16.
- [24] Mascolo G, Comparelli R, Curri ML, Lovecchio G, Lopez A, Agostiano A. Photocatalytic degradation of methyl red by TiO<sub>2</sub>: Comparison of the efficiency of immobilized nanoparticles versus conventional suspended catalyst. *Journal of Hazardous Materials*. 2007 Apr 2;142(1-2):130-7.
- [25] Jamali A, Vanraes R, Hanselaer P, Van Gerven T. A batch LED reactor for the photocatalytic degradation of phenol. *Chemical Engineering and Processing: Process Intensification*. 2013 Sep 1;71:43-50.
- [26] Hou D, Goei R, Wang X, Wang P, Lim TT. Preparation of carbon-sensitized and Fe–Er codoped TiO<sub>2</sub> with response surface methodology for bisphenol A photocatalytic degradation under visible-light irradiation. *Applied Catalysis B: Environmental*. 2012 Sep 25;126:121-33.